JOURNAL of ELECTROCHEMICAL SCIENCE and TECHNOLOGY

REVIEW

Progresses, Challenges and Prospects for Aluminum Anode in Aqueous Secondary Batteries

Keun-il Kim*

School of Chemical, Biological and Battery Engineering, Gachon University, Seongnam-si, Gyeonggi-do, 13120, Korea

ABSTRACT

Lithium-ion batteries (LIBs) dominate the current energy storage market, raising concerns about cost and safety. Due to their lower cost and enhanced safety, aqueous batteries are emerging as a prominent substitute to LIBs for grid-scale applications. Aluminum (Al) is the most abundant metal element in the Earth's crust, offering the merits of high theoretical capacity, safety, and low production cost. However, challenges such as a narrow electrochemical stability window (ESW) and hydrogen evolution reaction (HER) in aqueous electrolytes need to be properly addressed to achieve the practical use of aqueous batteries. This paper aims to summarize the history and progress of Al metal anodes in energy storage, followed by suggested potential pathways for the development of practical aqueous Al batteries.

KEYWORDS

Aqueous batteries, Aqueous aluminum-ion batteries, Aluminum anode, Solid-electrolyte interphase

CORRESPONDENCE
T: +82-31-750-8942
E: keunilkim@gachon.ac.kr
https://doi.org/10.33961/jecst.2024.00752

VOLUME 16 ISSUE 1 FEBRUARY 2025

RECEIVED 15 July 2024 ACCEPTED 24 September 2024

OPEN ACCESS This is an open-access article distributed under the terms of the Creative Commons Attribution Non-Commercial License (http://creativecommons.org/licenses/by-nc/4.0) which permits unrestricted non-commercial use, distribution, and reproduction in any medium, provided the original work is properly cited.

INTRODUCTION

To meet the growing energy demand resulting from rapid population growth and lifestyle changes, global power production is expected to reach 28 terawatts (TW) by 2050 [1–3]. Non-renewable fossil energy sources constitute a major portion of current electricity generation, raising concerns about carbon dioxide (CO_2) emissions and climate change. The ongoing transition in energy production aims for carbon neutrality to mitigate the accumulated environmental damage. In this regard, by 2050, renewable energies such as solar, wind, and hydropower are expected to account for over 85% of global electricity generation [4–7]. Utilizing these energy sources comes with the following limitations: 1) electricity generation is intermittent; 2) power must be converted to electricity for storage or transport; and 3) geopolitical conflicts can potentially result in unequal access to energy sources and disruptions to the global energy supply chain. To address these issues, global demand for gigawatt (GW)-scale grid infrastructure for energy storage is soaring, which can effectively store or supply electricity generated from sustainable energy sources. As a result, the global stationary energy storage market size is expected to exceed $535 billion by 2033, with a compound annual growth rate (CAGR) of 8.05% between 2024 and 2033 [8].

The conversion of generated electricity into various forms, such as pumped hydropower [5], flywheels [7], molten salts [9], capacitors [10], or chemical storage [11], is essential for energy storage. Among these options, batteries are emerging as key technologies due to their compatibility with both mobile and stationary platforms [6].

Depending on the application, key metrics of batteries must first be clearly distinguished [12]. Broadly, batteries can be categorized as either power or storage batteries, with a comparison of the desired performance for each depicted in Fig. 1.

State-of-the-art LIBs represent power batteries used for electrified transportation and portable electronics [13]. Since their main applications are in powering electric vehicles (EVs), customers and the market demand power batteries with extended driving ranges and fast-charging capabilities. Nonetheless, the constraints of high cost and safety concerns make the compatibility of LIBs questionable.

The key requirements for storage batteries are distinct from those of power batteries. Storage batteries, commonly referred to as energy storage systems (ESSs), are used to temporarily store electricity generated from sustainable sources on a grid scale. Storage batteries do not require high power density or fast-charging capabilities; instead, ensuring safety and reducing the levelized cost of energy (LCOE) [14] are the crucial evaluation metrics.

Electrolytes, which serve as ion-transport mediums in batteries, contribute significantly to the safety concerns of current battery technologies [15–17]. For high-voltage operations, aprotic organic solvents such as carbonates and ethers are widely used as electrolytes in LIBs due to their wide electrochemical stability

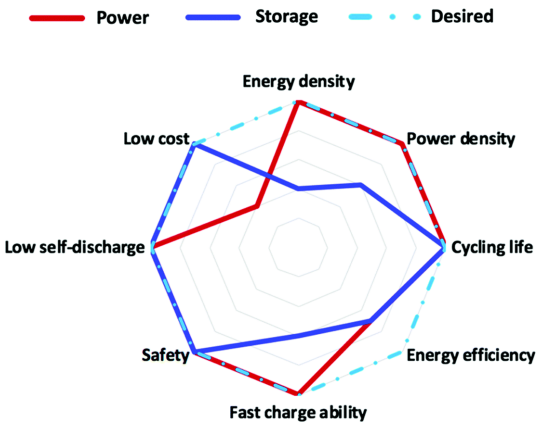

Fig. 1. Radar chart showing the required performance in comparison with the ideal cases, where red is for power batteries and blue is for storage batteries; the dashed light-blue line of the octagon marks the ideal scenarios. Reprinted from Ref. [12] with permission. Copyright 2019, the Royal Society of Chemistry.

window (ESW). However, the thermal and chemical instability of organic solvent-based electrolytes can lead to the generation of toxic, flammable gases, which can cause battery explosions. While the safety issues of LIBs have been tentatively addressed by manipulating the architecture of battery modules on the scale of portable power batteries, the feasibility of this approach remains uncertain for grid-scale ESSs [18–21].

Recent efforts to address the potential safety risks in LIBs focus on electrolyte modifications, including the addition of flame-retardant solvents [22,23]; the use of molten salts as electrolytes, such as ionic liquids or deep eutectic solvents [24,25]; the development of solid-state or gel-polymer electrolytes [26–28]; and the substitution of organic solvents in electrolytes with water [29,30]. However, the electrochemical decomposition of liquid electrolytes remains inevitable [31–33], and solid-state electrolytes suffer from dendritic Li deposition due to poor interfacial contact between the electrode and electrolyte [34].

Toxic, flammable gases generated by the decomposition of organic compounds and short circuits from dendritic deposition of Li [35–37] can trigger thermal runaway of batteries, leading to explosions. In contrast, aqueous electrolytes offer a safety advantage, as the decomposition products are primarily composed of non-flammable water vapor. Therefore, aqueous electrolytes garner substantial attention for their applications in ESSs, where safety is the predominant requirement.

A major drawback of aqueous electrolytes is their narrow electrochemical stability window (ESW) of 1.23 V. Demonstrations of aqueous LIBs have addressed this issue by widening the ESW of aqueous electrolytes through a high concentration of salts, known as water-in-salt electrolyte (WiSE) [29,30]. The ESW in WiSE is kinetically extended to 3 V, but the question remains whether the levelized cost of energy (LCOE) for aqueous LIBs can be competitive for grid-scale applications. Consequently, recent efforts have been devoted to searching for feasible metallic charge carriers beyond lithium.

Amid potential metallic charge carriers for aqueous batteries, zinc (Zn) has been the most actively investigated due to its high volumetric capacity, compatible redox potential of –0.76 V vs. SHE, and low production cost (Table 1) [38–40]. Aluminum, being the most abundant metal in the Earth's crust and the third most abundant element overall, offers a competitive production cost compared to Zn. This cost could potentially be reduced further due to already well-established mining, processing, and recycling industries for Al metal [41,42]. Moreover, Al has high volumetric and gravimetric capacities via a 3-electron exchange redox process (2,980 mAh g^{-1} and 8,046 mAh cm^{-3}).

Since Sony's first commercial introduction of carbon-based negative electrode [43,44], intercalation-based materials, such as carbonaceous compounds [45], metal oxides [46], dominate the anode market in LIBs. Repeated (de) intercalation of monovalent Li-ions causes minimal strain to the anode's crystal lattice; thereby allowing stable performance of anode in long-term cycling. On the other hand, storage kinetics and structural stability of the hosts are deteriorate during the intercalation of multivalent metallic charge carriers (*e.g.*, Ca^{2+}, Mg^{2+}, Zn^{2+}, and Al^{3+}, etc.) with high charge density. For instance, the first investigation on intercalation-type anode for aqueous Al-ion batteries in 2015 reported limited capacity, 25 mAh g^{-1}, in TiO_2 nanotube arrays [47], and the study of Das et al. used graphene-decorated anatase TiO_2 anode with Al^{3+} storage

Table 1. Comparison of standard potential (V vs. Standard Hydrogen Evolution, SHE), ionic radius, theoretical capacity, abundance in the Earth's crust and cost of typical metallic charge carriers

Charge Carriers	Standard Potential (V vs. SHE)	Ionic Radius (Å)	Theoretical Capacity		Abundance in the Earth's crust (ppm)	Cost ($ lb^{-1})
			Gravimetric (mAh g^{-1})	Volumetric (mAh cm^{-3})		
Li	–3.04	0.76	3,862	2,062	17	8–11
Na	–2.71	1.02	1,166	1,128	23,000	1.1–1.6
K	–2.92	1.38	686	610	15,000	3–9
Mg	–2.36	0.72	2,205	3,833	29,000	1–1.5
Ca	–2.86	1.00	1,340	2,073	50,000	-
Zn	–0.76	0.74	820	5,851	79	0.5–1.5
Al	–1.67	0.54	2,980	8,046	82,000	0.5–1.5

capacity of 33–50 mAh g^{-1} [48]. Later the same group revealed MoO_3 showed improved Al^{3+} storage capability with the initial reversible capacity of *ca*. 500 mAh g^{-1} in 1 M $AlCl_3$ aqueous electrolyte, but rapid capacity fading was observed where the capacity dropped below 200 mAh g^{-1} in early stage of cycling [49].

To fully utilize the merits of metallic charge carriers in their high theoretical capacity and energy density, it is clear that future studies must take the strategic approaches in employing metals themselves as the anode in rechargeable batteries. For aqueous multivalent-ion batteries, in particular, intercalation-based anode materials become less competitive due to structural instability and high desolvation energy barrier of charge carriers from hydrated complexes.

Therefore, akin to the field of aqueous Zn batteries, profound understanding on the reaction mechanism of Al metal anode in aqueous batteries must be established, followed by the clear demonstration of the challenges to be overcome, so that the above-mentioned advantages of Al metal in energy storage can be realized as the potential alternative to LIBs. This review aims to provide an outlook on the progress, challenges, and prospects of Al metal anodes in aqueous secondary batteries.

PROGRESSES AND CHALLENGES FOR AL METAL ANODE IN AQUEOUS BATTERIES

History of Al metal anode in energy storage

The application of aluminum (Al) in energy storage dates back to 1855, when Hulot demonstrated a primary cell composed of an Al cathode and a Zn–Hg amalgam anode in a diluted sulfuric acid electrolyte [50]. Al was first employed as an anode in the Buff cell in 1857 [51], and later, an amalgamated Al–Zn alloy was used as an anode with a carbon cloth cathode [52]. Limited success was reported with Al metal anodes [53–55] until the Archer group revealed the first reversible electrochemical charge storage system using a pristine Al foil anode paired with a V_2O_5 nanowire cathode in an ionic liquid (IL) electrolyte composed of $AlCl_3$ and 1-ethyl-3-methylimidazolium chloride ([EMIm]Cl) [56]. In a subsequent study, Dai et al. reported a rechargeable Al-graphite battery with an AlCl3/[EMIm]Cl IL electrolyte [57]. Non-flammable, room-temperature ILs enabled reversible plating/stripping of Al by partially corroding the surface-passivating oxide film on the Al anode, while the cathode stored charge via anion intercalation chemistry, such as $AlCl_4^-$. However, the storage of bulky tetrachloroaluminate anions sacrifices the specific capacity of graphitic cathodes (≤100 mAh g^{-1}). Consequently, active research has been conducted to explore suitable cathode materials, including organic compounds, metal chalcogenides, sulfur, and carbon materials, to increase the cycle life and capacity of IL-based Al batteries [58–61].

Despite their merits, the practical application of IL-based electrolytes is hindered by two major issues: 1) ILs are sensitive to atmospheric moisture, requiring that electrolyte synthesis and cell assembly be performed in inert atmospheres, and 2) ILs, which are strongly acidic to corrode the passivating Al_2O_3 layer on the surface, are highly corrosive and limit the selection of current collectors to expensive metals, such as Ti and Mo. To reduce overall production cost and fully utilize the high theoretical capacity of Al^{3+}/Al redox, the development of aqueous electrolytes for rechargeable aluminum metal batteries (AMBs) has emerged.

Reaction mechanism and issues of Al metal anode in aqueous electrolytes

As mentioned in the previous section, reversible plating/stripping of Al on metal foil is enabled by the corrosion of the surface aluminum oxide layer and the reversible redox reaction between two anionic species, $Al_2Cl_7^-$ and $AlCl_4^-$ [58–61]. Note that aluminum ions do not exist as Al^{3+} in ionic liquids (ILs); instead, they exist in the form of $Al_2Cl_7^-$. Therefore, a profound understanding of the solvation structure of Al^{3+} in an aqueous medium and the reaction mechanism is necessary.

In aqueous solutions, trivalent aluminum cations, with extremely high Lewis acidity, form a solvation shell with six water molecules, $[Al(H_2O)_6]^{3+}$ [62]. As depicted in Fig. 2a, the standard reduction potential of Al (–1.67 V vs. SHE) is significantly lower than the hydrogen evolution reaction (HER) potential.

To suppress the activity of water and expand the ESW of aqueous electrolytes, efforts have been dedicated to developing high-concentration aqueous electrolytes with various salts, such as aluminum nitrate ($Al(NO_3)_3$), aluminum sulfate ($Al_2(SO_4)_3$), and aluminum trifluoromethanesulfonate ($Al(Otf)_3$) (Fig. 2b) [63]. Unlike WiSE for aqueous Li-ion batteries, in which 21 *m* of lithium bis(trifluoromethane)sulfonimide (LiTFSI) salt is dissolved, the highest concentration of Al salts reported so far is 5 *m* $Al(Otf)_3$ [64,65]. Even in a saturated aqueous solu-

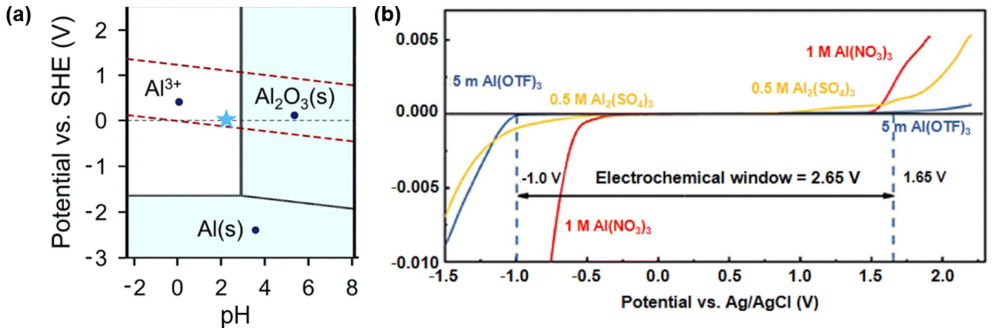

Fig. 2. (a) Pourbaix diagram of 1 M Al at 25°C. Reprinted from Ref. [62] with permission. Copyright 2022, the Royal Society of Chemistry. (b) Linear sweep voltammetry (LSV) of aqueous electrolytes on Ti mesh in a three-electrode system at 10 mV s^{-1} using electrolytes of 5 M $Al(Otf)_3$, 1 M $Al(NO_3)_3$, and 0.5 M $Al_2(SO_4)_3$, respectively. Reprinted from Ref. [63] with permission. Copyright 2024, the Royal Society of Chemistry.

tion with 5 *m* $Al(Otf)_3$, HER is triggered at around –1.0 V vs. Ag/AgCl, leaving approximately a 1 V gap from the standard reduction potential of Al (–1.85 V vs. Ag/AgCl).

Not only is the solubility of Al salts too low to constitute an anion-coordinated solvation sheath around Al ions, but the partial transfer of electrons from coordinated water molecules to the aluminum ion's empty orbital weakens the O–H bonds in water and promotes HER in aqueous solutions [66–68]. H_2 gas evolution on the metal surface increases the local pH by the accumulation of OH^-, inducing the continuous build-up of insulating oxide layers, such as Al_2O_3. It must be realized that aside from the desired redox reaction of $Al^{3+} + 3e^- \leftrightarrow Al$, the redox pathways of Al in an aqueous medium are complicated by various side reactions.

$$Al^{3+} + 3e^- \leftrightarrow Al \quad (1)$$

$$H_2O \leftrightarrow H^+ + OH^- \quad (2)$$

$$2OH^- \leftrightarrow O^{2-} + H_2O \quad (3)$$

$$2Al^{3+} + 3O^{2-} \leftrightarrow Al_2O_3 \quad (4)$$

$$Al_2O_3 + 3H_2O \leftrightarrow 2Al(OH)_3 \quad (5)$$

$$Al(OH)_3 + H^+ \leftrightarrow Al(OH)_2^+ + H_2O \quad (6)$$

$$Al(OH)_2^+ + 2H^+ \leftrightarrow Al^{3+} + 3H_2O \quad (7)$$

$$Al(OH)_2^+ \leftrightarrow AlOOH + H^+ \quad (8)$$

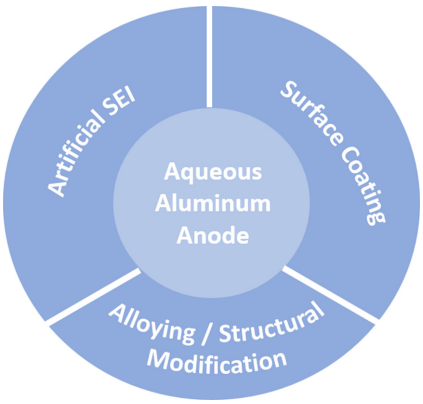

Fig. 3. Schematic illustration on the reported strategies to stabilize Al anode in aqueous electrolytes.

Such inherent side reactions result in a high overpotential for Al plating/stripping, poor cyclability, and a limited cycle life for the Al anode [69,70]. Therefore, anode-electrolyte interfacial engineering must accompany the development of suitable electrolytes to overcome the kinetic barriers in Al plating/stripping with an Al metal anode. The following section introduces the progress of Al anodes in aqueous batteries from different aspects: surface coating, artificial SEI formation, and alloying/structural modification (Fig. 3).

Progresses in anode modification for aqueous Al batteries

Surface coating

Surface coating is a simple yet effective strategy to prevent direct contact between water and the metal surface, thereby suppressing undesirable side reactions. Polymers are widely used as protective coatings on metal anode surfaces in aqueous electrolytes. An early study on aqueous Zn batteries reported that highly

polar β-phase poly(vinylidene difluoride) (PVDF) serves as a bifunctional coating material. The hydrophobic PVDF keeps water molecules away from the Zn surface, and PVDF molecules aligned in a trans-configuration on the surface guide the selective transport of Zn^{2+} for uniform deposition [71].

Taking advantage of the PVDF polymeric protective coating in aqueous Zn batteries, the Li group applied the β-PVDF coating to an Al foil anode (PVDF–Al) (Fig. 4a) [72]. HER potential of PVDF–Al was recorded at 0.08 V (vs. Al/Al^{3+}), whereas HER begins at 0.51 V (vs. Al/Al^{3+}) for pristine Al foil, indicating the effectiveness of the PVDF coating in suppressing HER (Fig. 4b). Fig. 4c depicts the comparison of corrosion current measurements using linear polarization curves. PVDF–Al showed a lower corrosion potential (1.02 V vs. Al/Al^{3+}) and corrosion current (1.32 mA cm^{-2}) than bare Al (1.15 V vs. Al/Al^{3+} and 1.78 mA cm^{-2}, respectively). This clearly demonstrates the improved corrosion resistance of the Al foil with the functional PVDF coating. As a result, the long-term cyclability of PVDF–Al is enhanced at a current density of 0.1 mA cm^{-2} (Fig. 4d).

Stabilization of Al anode with PVDF was further evaluated in full-cell set up with $K_2CoFe(CN)_6$ cathode. Decent average discharge voltage of *ca.* 1.0 V and the initial reversible capacity of 60 mAh g^{-1} was observed from galvanostatic charge/discharge (GCD) curves (Fig. 4e). With reduced side reactions on the anode surface, $K_2CoFe(CN)_6$ ‖ PVDF–Al full-cell demonstrated stable cycling over 400 cycles, where $K_2CoFe(CN)_6$ ‖ bare Al cell failed after 250 cycles.

MXene, a 2D material with various functional groups, has been widely adopted for protective coatings in energy storage due to its chemical and mechanical integrity as well as high electrical conductivity [73–75]. Yu *et al*. reported the self-assembly of a MXene thin film on the surface through charge exchange interac-

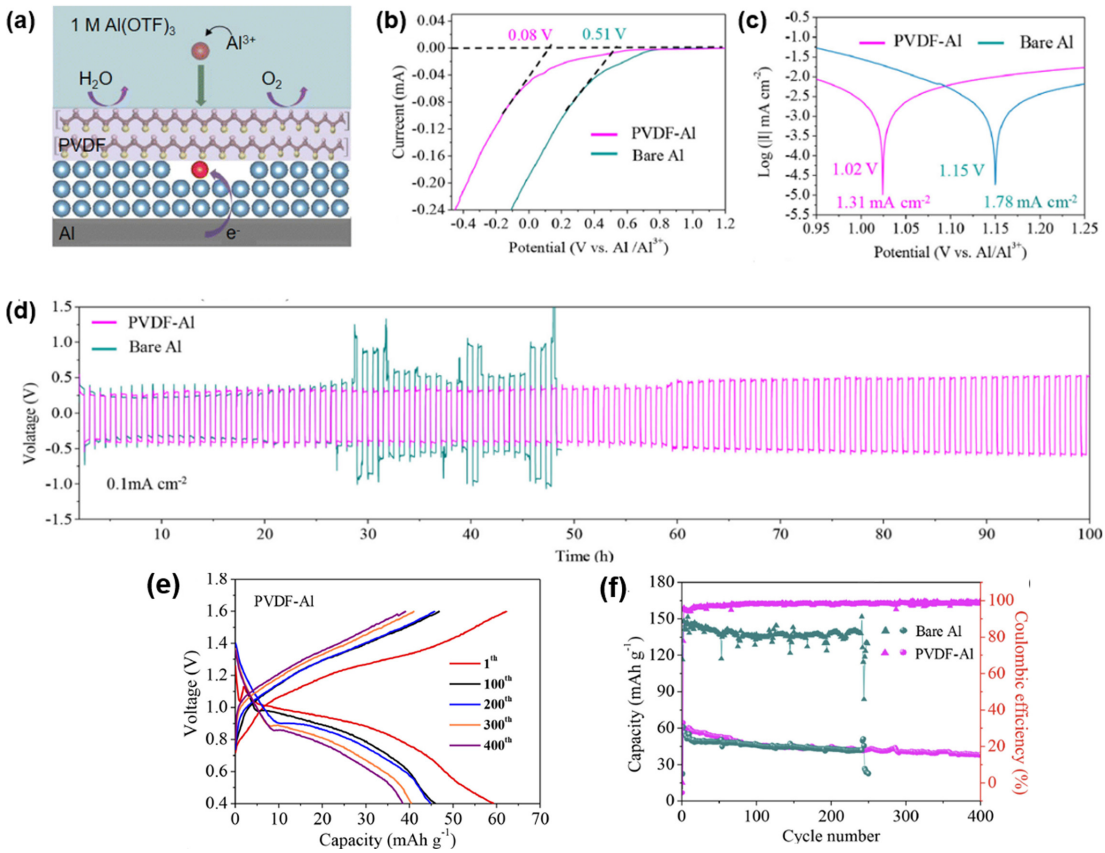

Fig. 4. (a) Schematic illustration of diffusion pathways of Al^{3+} across the PVDF coating. (b) LSV curves of bare and PVDF–Al. (c) Linear polarization curves for bare Al and PVDF–Al. (d) Long-term galvanostatic cycling results of Al ‖ Al symmetric cells with 1 M $Al(OTF)_3$ solution at 0.1 mA cm^{-2}. (e) GCD curves of $K_2CoFe(CN)_6$ ‖ PVDF–Al full-cells at 0.1 A g^{-1}. (f) Long-term cycling performance of $K_2CoFe(CN)_6$ with Al and PVDF–Al anodes. Reprinted from Ref. [72] with permission. Copyright 2022, Elsevier.

tions between Al^{3+} and the oxygen-containing functional groups of MXene, with the thickness of the MXene layer adjustable by regulating the reaction time (Fig. 5a) [76]. Reduced voltage hysteresis between plating and stripping of Al was observed in cyclic voltammetry (CV) with the optimized thickness of the MXene film (MAl-80), indicating improved kinetics via the conductive coating (Fig. 5b). Fig. 5c further illustrates the reduced nucleation overpotential of 49 mV for MXene-coated Al foil, compared to 112 mV for bare Al foil. The MXene coating improved interfacial kinetics with low overpotential during the plating/stripping of Al, along with stable protection, as demonstrated by the long-term cycling performance of MAl ‖ MAl symmetric cells (Fig. 5d).

With its capability to accept four electrons via sequential reduction, the organic cathode, pyrene-4,5,9,10-tetraone (PTO) was chosen as the cathode in this study for evaluating full-cell performance. Even with a high-mass loading cathode (~15 mg), the PTO ‖ MAl-80 full-cell achieved reversible capacity close to 300 mAh g^{-1} with a low overpotential (0.45 V), attributed to the improved conductivity of MAl-80 anode (Fig. 5e). Moreover, the prevention of side reactions via MXene coating was illustrated by the superior long-term cycling performance of MAl-80 compared to the full-cell with a bare Al anode (Fig. 5f).

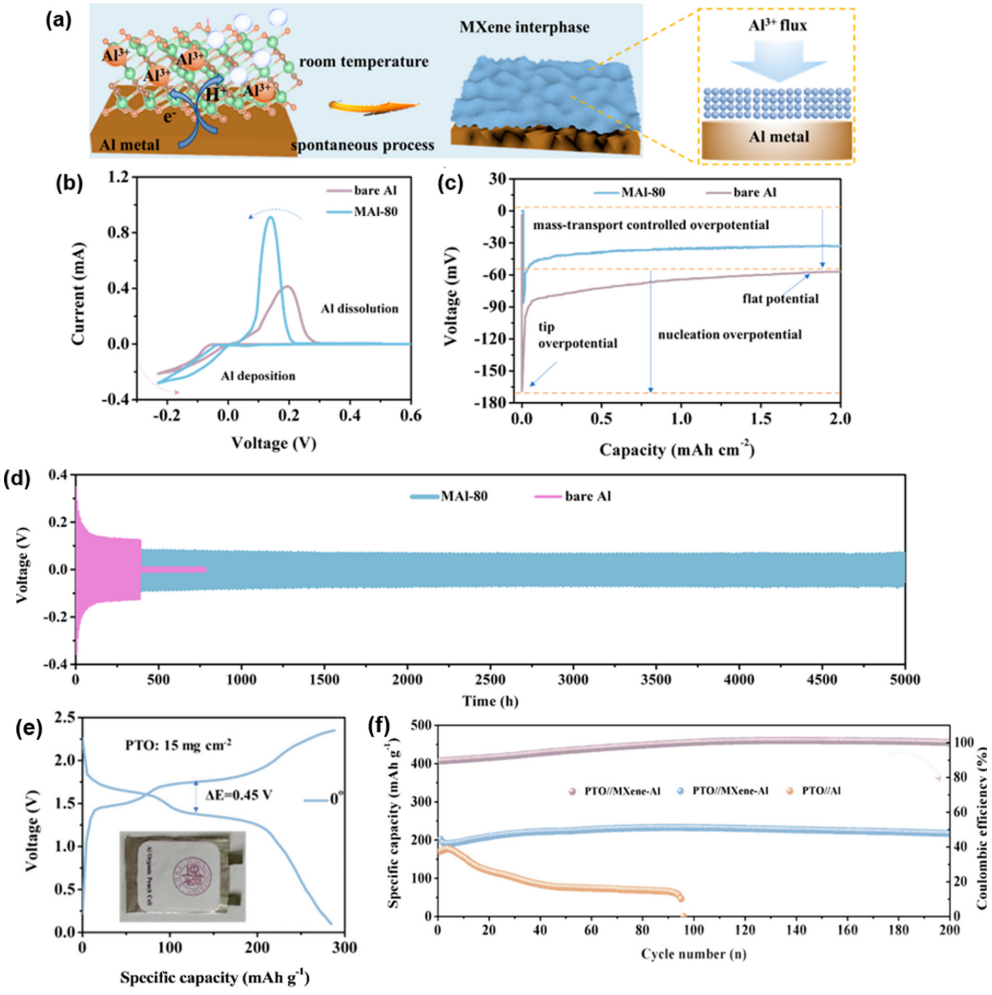

Fig. 5. (a) Schematic illustration of the MXene hybrid interphase on Al foil. (b) Cyclic voltammetry (CV) curve of Al plating/stripping at 0.1 mV s^{-1}. (c) Voltage hysteresis at current densities of 1 mA cm^{-2}. (d) Comparison of cycling performance of bare Al and MAl-80 at 12 mAh cm^{-2}. (e) GCD curve of PTO ‖ Al at 0.1 A g^{-1}. (f) Long-term cycling performance at 1 A g^{-1} after 200 cycles. Reprinted from Ref. [76] with permission. Copyright 2023, American Chemical Society.

Artificial solid electrolyte interphase (SEI)

Exposed to atmospheric oxygen and water, a passivating Al_2O_3 layer readily forms on the surface of Al due to the high charge density and strong oxide bonding energy of trivalent aluminum ions. In aqueous electrolytes, the nucleation of Al involves the electrochemical decomposition of water; hence, the continuous formation of the aluminum oxide layer becomes inevitable, rendering the surface electrochemically inert. IL-based electrolytes have achieved satisfactory cycle life with Al_2O_3-passivated Al anodes, so a profound understanding of the interfacial reaction mechanisms in ILs could provide valuable insights into how to keep Al "active" for reversible electrodeposition in aqueous media.

As illustrated in Fig. 6, Archer *et al*. proposed a simple strategy to construct an artificial SEI on Al foil by dipping it in an $AlCl_3$-[EMIm]Cl IL electrolyte (the treated Al is denoted as TAl) [77]. Fourier transform infrared spectroscopy (FTIR) results indicate the formation of an SEI enriched with functional groups such as C=O, C=C, and C=N, derived from the interaction between Al and the IL. Additionally, Cl- and N-rich SEI formation was detected using cross-sectional scanning electron microscopy (SEM) and energy-dispersive X-ray spectroscopy

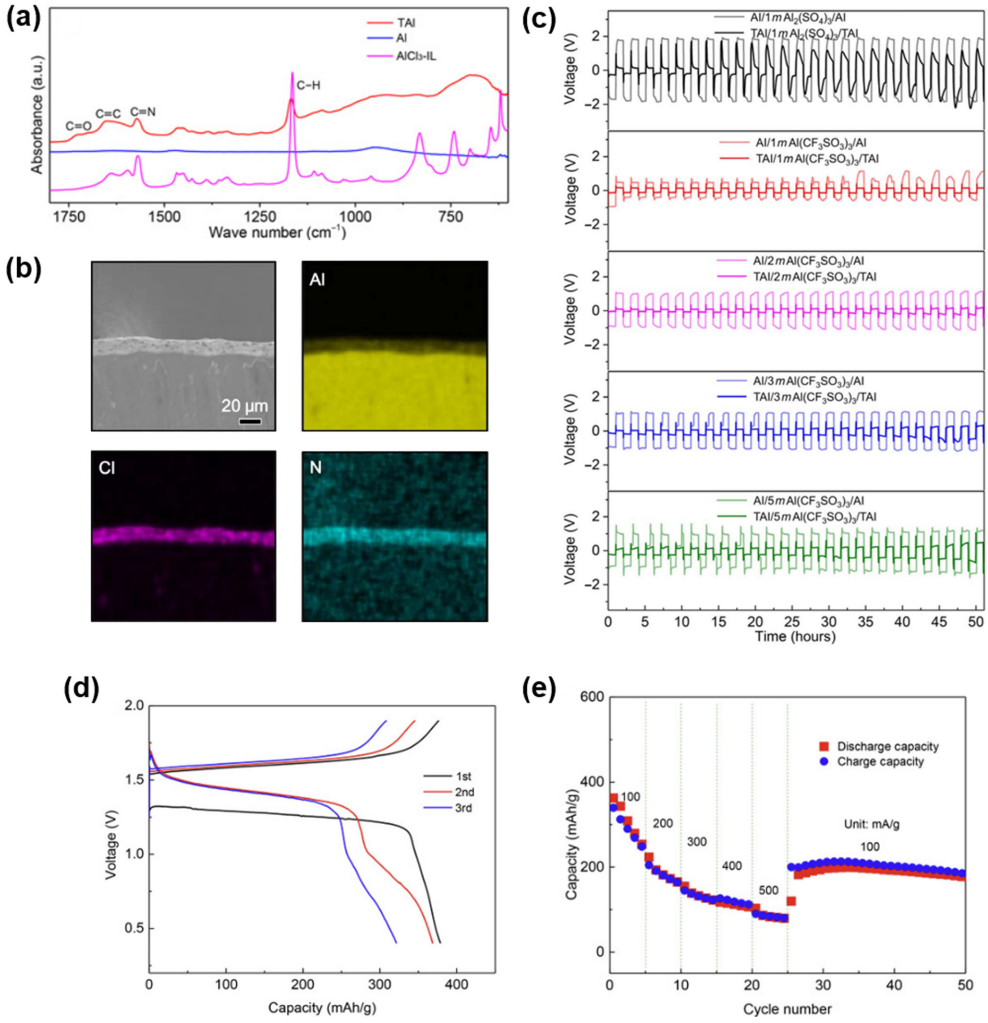

Fig. 6. (a) ATR-FTIR spectra of Al and TAl foil. (b) Cross-sectional SEM image of a TAl foil and corresponding EDX mapping of Al, Cl, and N. (c) Al ‖ Al symmetric cell tests using Al and Tal coupled with different electrolytes at the current density of 0.2 mA cm^{-2}. (d) GCD curves of aqueous MnO_2 ‖ TAl batteries at 100 mA g^{-1} in 2 *m* $Al(Otf)_3$. Reprinted from Ref. [77] with permission. (e) Rate performance of MnO_2 ‖ Tal. Copyright 2018, American Association for the Advancement of Science.

(EDX) (Fig. 6a,b). Participation of imidazolium in the SEI formation via ring-opening reaction was also evidenced from reduced signal in the vibration mode of C–H bond after the treatment. Due to the corrosion of the passivating oxide layer and improved ion-transport kinetics through the artificial SEI, low voltage hysteresis in the plating/stripping of TAl was observed in aqueous electrolytes (Fig. 6c).

Fig. 6d,e demonstrate α-MnO_2 ‖ TAl full-cell performance in 2 *m* $Al(Otf)_3$ electrolyte. GCD curves of a full-cell showed the energy density equivalent to 500 Wh kg^{-1} with a specific capacity of 380 mAh g^{-1} and an average discharge voltage of ~1.3 V (Fig. 6d). However, the stability of artificial-SEI on TAl remains questionable as witnessed with rapid capacity decay and limited cycle life of 50 cycles or less (Fig. 6e). Subsequent studies focused on enhancing the stability of the artificial SEI and reducing costs by replacing [EMIm]Cl with different precursors, including acetamide [78] and urea [79].

Alloying and structural manipulation of Al metal

Manipulating the solvation structure of aluminum ions extends the ESW of aqueous electrolytes to some extent, but the nucleation potential of aluminum remains far below the HER threshold, even in saturated electrolytes [63]. Underpotential deposition (UPD) of metals describes the positive potential shift during the electrodeposition of a metal on other metal substrates through the reversible formation of intermetallic phases [80–82]. Consequently, investigations into substrates capable of forming Al-metal alloys have been actively conducted in recent years.

In 2020, the Yu group prepared an Al pre-intercalated MnO_2 cathode, with Zn serving as a substrate via the

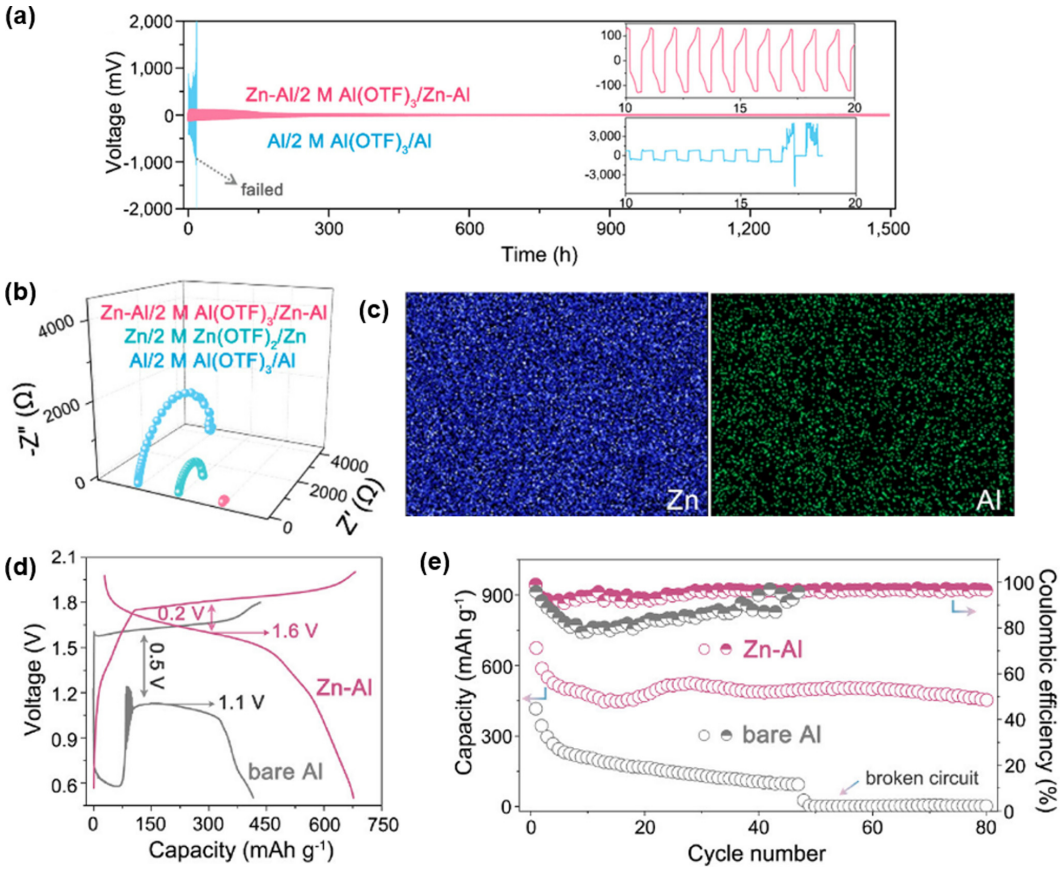

Fig. 7. (a) Voltage profiles for symmetric cells based on Zn and Al substrates in 2 M $Al(OTF)_3$ electrolyte at 0.2 mA cm^{-2}. (b) Comparative Nyquist plots symmetric cells. (c) EDX mappings from the top view of the Zn–Al anode. (d) First GCD curves of MnO_2 ‖ Zn–Al and MnO_2 ‖ bare Al full cell. (e) Cycling performance of MnO_2 ‖ Zn–Al full cell at 100 mA g^{-1}. Reprinted from Ref. [83] with permission. Copyright 2022, American Chemical Society.

reversible formation of a Zn–Al alloy in 2 M $Al(Otf)_3$ aqueous electrolyte [83]. A continuous increase and abrupt fluctuations in the voltage profile are conspicuous in the Al ‖ Al symmetric cell; meanwhile, polarization in the Zn–Al cell remains stable at under 25 mV for 1,000 hours of cycling (Fig. 7a). Since the reduction of Zn^{2+} occurs prior to Al^{3+}, Al ions provide electrostatic shielding on the surface of the Zn substrate during the plating/stripping of Zn. Moreover, the co-deposition of Zn^{2+} and Al^{3+} via alloying significantly lowers the energy barrier for the nucleation of Al (Fig. 7b). The absence of metallic Al or an aluminum oxide layer in the X-ray diffraction (XRD) patterns, along with the homogeneous elemental distribution of Zn and Al (Fig. 7c), demonstrates that Al^{3+} is completely plated in the form of a Zn–Al alloy. A full-cell was demonstrated with Al preloaded in MnO_2 (Al_xMnO_2) as the cathode and Zn as the alloy-forming substrate in 2 M $Al(Otf)_3$ electrolyte, which showed a high discharge voltage plateau at 1.6 V, with the initial capacity exceeding 675 mAh g^{-1} (Fig. 7d), and a reversible capacity of 460 mAh g^{-1} was well maintained after 80 cycles (Fig. 7e).

In a later study, Jiang *et al*. introduced the lamella-nanostructured eutectic $Al_{82}Cu_{18}$ alloy (E-$Al_{82}Cu_{18}$) electrode for aqueous Al-ion batteries [84]. The eutectic alloying during the synthesis created phase separation, composed of Al_2Cu lamellas and α-Al lamellas. The alternating α-Al and Al_2Cu nano-lamellar structure was confirmed through EDX elemental mapping, as shown in Fig. 8a. The more-noble Al_2Cu nano-lamellas facilitate the transport of electrons and promote homogeneous plating/stripping, while Al-ions are supplied by the electroactive α-Al. The phase-segregated Al–Cu alloy exhibited stable long-term plating/stripping performance at various current densities (Fig. 8b). Fig. 8c illustrates the electrochemical impedance spectroscopy (EIS) spectra; a significantly low charge transfer resistance of E-$Al_{82}Cu_{18}$ was measured (~160 Ω) due to suppressed formation of thick oxide layers and the synergistic effect of α-Al/Al_2Cu galvanic couple.

Eutectic nano-lamellas enabled selective redox of Al with improved kinetics, as observed from the significantly reduced overpotential in Al_xMnO_2 ‖ E-$Al_{82}Cu_{18}$ full-cell (Fig. 8d). The improvement of reversible Al plating/stripping capability in the full-cell demonstration contributes to a remarkable capacity retention of 83% after 400 cycles (Fig. 8e).

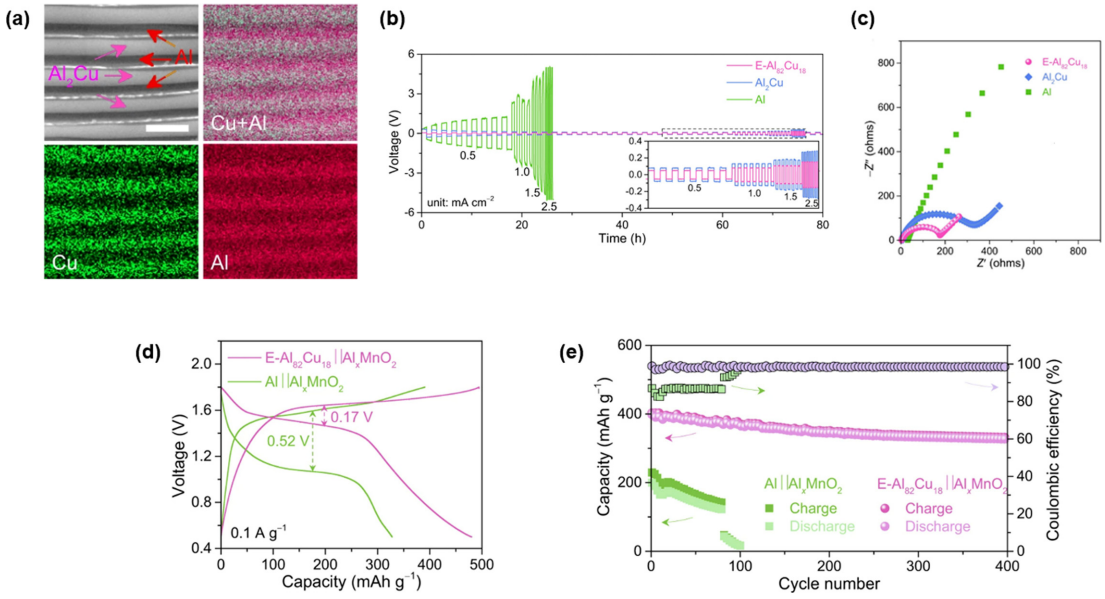

Fig. 8. (a) SEM backscattered electron image of E-$Al_{82}Cu_{18}$ with different contrasts corresponding to α-Al and intermetallic Al_2Cu lamellas, and EDX elemental mapping of Cu (in green) and Al (in red). Scale bar, 1 μm. (b) Comparison of rate performance for symmetric cells of E-$Al_{82}Cu_{18}$ (pink line), Al_2Cu (blue line), and Al (green line) at various current densities (inset: enlarged voltage-time profiles). (c) EIS spectra of E-$Al_{82}Cu_{18}$ (pink spheres), Al_2Cu (blue diamonds), and pure Al (green squares) symmetric cells. (d) GCD profiles of Al_xMnO_2 ‖ E-$Al_{82}Cu_{18}$ (pink line) and Al_xMnO_2 ‖ Al (green line) cells at the specific current of 0.1 A g^{-1}. (e) Comparison of rate performance and Coulombic efficiency for Al_xMnO_2 ‖ E-$Al_{82}Cu_{18}$ (pink spheres) and Al_xMnO_2 ‖ Al cells (green squares), which are performed at various specific currents from 0.1 to 5 A g^{-1}. Reprinted from Ref. [84] with permission. Copyright 2022, Springer Nature.

Amorphous or glassy metals, unlike crystalline metals, lack long-range atomic arrangements in their structure [85,86]. The disruption in the interstitial sites of glassy metals imparts exceptional properties, such as excellent oxidation resistance and a low diffusion rate of oxygen within the structure. Another interesting feature of glassy metals is the positive shift in the electrodeposition potential, as described in UPD, due to their higher reactivity compared to crystalline metals [87–89]. To investigate whether structural amorphization could stabilize the Al anode in aqueous electrolytes, Yu and co-workers conducted the amorphization of Al metal (Al@*a*-Al) via (de)alloying with Li ions (Fig. 9a) and examined its performance in aqueous Al batteries [90].

Once electrochemically plated Li is stripped (Al@*a*-Al), a distinct boundary between the amorphous and the crystalline phases is created (Fig. 9b). Restrained corrosion in glassy Al@*a*-Al was confirmed by a normalized corrosion current density approximately 400 times lower than that of pristine Al foil, indicating sluggish HER kinetics (Fig. 9c). As shown in the cyclability comparison of symmetric cells in Fig. 9d, Al@*a*-Al outperforms the bare Al anode in terms of durability and voltage hysteresis. It is also noteworthy that this study employed an aqueous electrolyte with low-cost $Al_2(SO_4)_3$ salt instead of expensive $Al(Otf)_3$-based electrolytes, highlighting the potential for structural modification of Al metal in large-scale applications.

Potassium nickel hexacyanoferrate (KNHCF) is one of the promising cathode candidates for hosting Al-ions due to its structural integrity for long-term cycling. Disordered orientation in amorphous region enhanced the kinetics of Al plating/stripping, as shown by high open-circuit voltage and the average discharge potential in KNHCF ‖ Al@*a*-Al full-cell (Fig. 9e) with dramatic enhancement in cyclability (Fig. 9f).

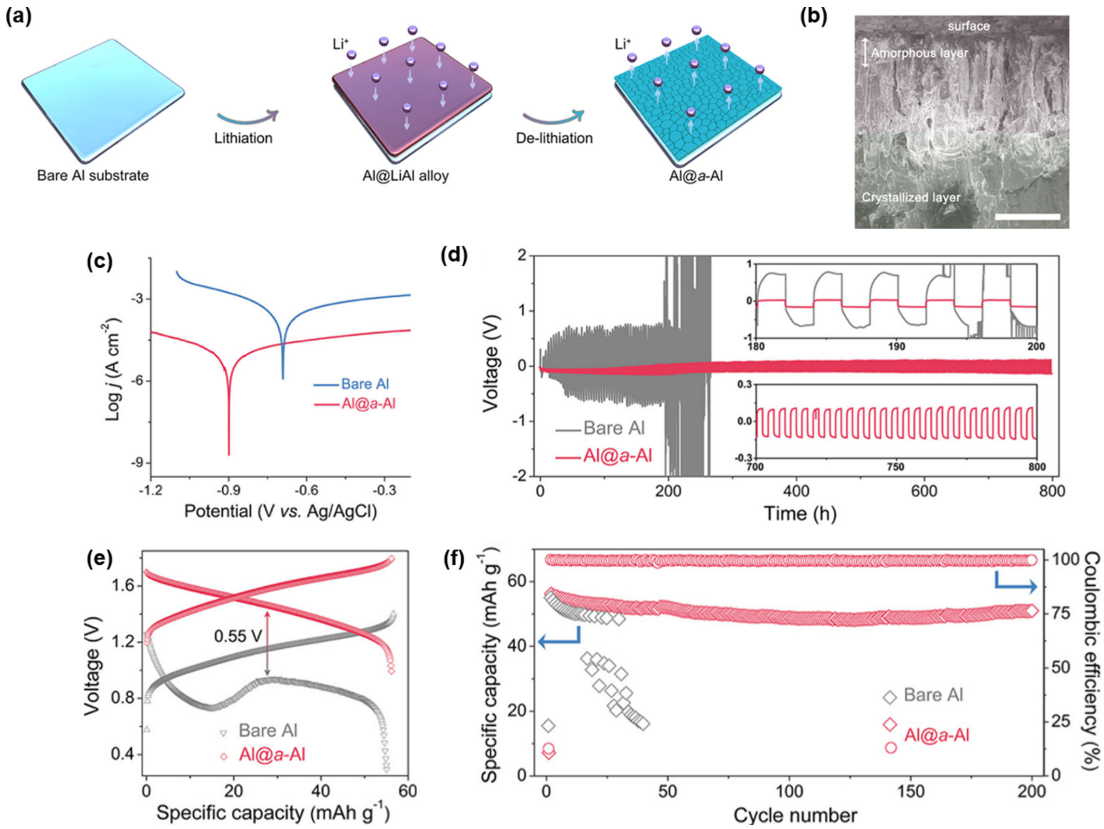

Fig. 9. (a) Schematic illustration of the design and preparation of the Al@*a*-Al anode. (b) SEM image of the cross section of the Al@*a*-Al anode. (c) Potentiodynamic polarization curves normalized by the electrochemical active surface area (ECSA) of bare Al (blue) and Al@*a*-Al (red). (d) Comparison of voltage profiles for symmetric cells: bare Al (grey); Al@a-Al (red) in 0.5 M $Al_2(SO_4)_3$ at 0.05 mA cm^{-2} for 2 h in each cycle. (e) GCD voltage profiles and (f) cycling performance comparison of of KNHCF ‖ Al@*a*-Al and KNHCF ‖ bare Al cells at a specific current of 100 mA g^{-1}. Reprinted from [90] with permission. Copyright 2022, American Chemical Society.

CONCLUSIONS AND PERSPECTIVES

Conclusions

The rapid expansion of the sustainable energy sector necessitates the development of cost-effective and safe energy storage solutions beyond conventional LIBs. Aluminum presents several key advantages, such as low cost, enhanced safety, and high theoretical capacity, positioning it as a strong candidate for grid-scale applications. Nevertheless, the development of aqueous Al batteries remains in its early stages, with current performance metrics—such as specific capacity and long-term cycling stability—falling short of the requirements for practical-scale deployment. To advance the viability of sustainable aqueous Al-metal batteries for grid-scale ESSs, several critical challenges must be addressed concurrently.

Surface modification & structural engineering of Al-metal anode

The presence of a native Al_2O_3 layer significantly limits the electrochemical activity of Al-metal anodes in aqueous batteries. Specifically, the continuous accumulation of a thick, electrically and ionically insulating oxide layer undermines the reversibility of Al plating/stripping. To maintain the electrochemical activity of Al-metal anodes in aqueous environments, future studies should focus on strategies to minimize the formation of Al_2O_3 on the surface.

The application of hydrophobic coating layers is one potential approach. While extended cycle life and improved electrochemical reversibility have been demonstrated for Al anodes, the underlying reaction mechanisms remain poorly understood. It is important to note that protective membranes with complex functional groups can impede the investigation of ion transport and diffusion mechanisms through the coating. Although surface coatings can stabilize the Al-electrolyte interface by physically separating Al from the aqueous electrolyte and mitigating the HER, questions remain about their impact on the kinetics of Al-ion transport. Future research should prioritize the exploration of hydrophobic, yet aluminophilic, compounds as candidates for surface coatings.

Studies on the pre-treatment of Al foil have demonstrated effective erosion of Al_2O_3 and the formation of an artificial SEI. However, ongoing debates exist regarding several aspects: i) the cyclability of Al with an artificial SEI showed minimal improvements, raising questions about the long-term stability of the SEI in aqueous media; ii) circumventing oxide layer passivation for Al redox has only been reported in Cl-rich environments, without a clear understanding of the underlying mechanisms. Even with a Cl-rich SEI, Al anode in aqueous electrolytes exhibited inferior performance, whereas the plating/stripping efficiency exceeded 99% for 7,500 cycles in an $AlCl_3$-[EMIm]Cl ionic liquid electrolyte. This leads to the question: What is the nature of the interaction between Cl^- and the surface oxide? Is the artificial SEI stable enough to provide long-term protection?

Since the introduction of the $AlCl_3$-[EMIm]Cl IL electrolyte for reversible Al plating/stripping, numerous studies have sought to elucidate the underlying reaction mechanisms, which may provide answers to the aforementioned questions. In 2014, Grady et al. investigated the interaction of Cl^- with the passive aluminum oxide film in ILs, reporting that Cl^- initially adsorbs and incorporates into the bulk oxide. Cl^- then migrates toward the metal-oxide interface through oxygen vacancies, thinning the oxide layer and inducing localized dissolution of the underlying Al [91]. Later studies revealed that Cl^- enhances the electrochemical performance of the Al anode in aqueous electrolytes primarily through a corrosion process rather than by promoting Al redox through SEI formation, as previously hypothesized [92]. For example, the electrochemical performance of pristine Al foil in 2 *m* $Al(Otf)_3$ electrolytes containing a small amount of chloride salt (0.15 *m* NaCl) was found to be comparable to that of pre-treated Al foil. The SEI is unstable and dissolves rapidly in water, rendering it incapable of preventing the continuous decomposition of water molecules in aqueous electrolytes [64]. Thus, it must be recognized that aggressive chloride ions are responsible for dissolving Al beneath the oxide layer, leading to low overpotentials for the anode. Furthermore, Cl^- is continuously consumed during repetitive corrosion, indicating that neither the formation of an “artificial SEI” nor the mere addition of a chloride-containing source can achieve long-term stabilization of the Al anode.

While a pre-formed SEI generated through IL treatment lacks long-term stability, it has shown promise in enhancing the electrochemical activity of aluminum metal. To address the instability of artificial SEIs in aqueous electrolytes, applying additional protective layers offers a potential solution. Hydrophobic coatings, such as PVDF, can improve the chemical stability of the SEI in aqueous environments, preserving the aluminum

anode's electrochemical performance.

In parallel, structural modifications like UPD offer another approach, allowing the use of alloy or glassy metal anodes by shifting the nucleation potential of aluminum. This method effectively suppresses HER, but at the expense of reduced energy density due to the mass of the alloying elements. Recent studies have also highlighted significant gas evolution during aluminum dissolution in Al–Cu and Al–Zn alloy anodes in aqueous batteries, raising concerns about the previously reported performance improvements of these alloyed systems [93].

To balance HER suppression with energy density, future research should focus on optimizing alloy compositions and structures. For instance, using lightweight alloying elements or dopants that enhance nucleation potential without adding substantial mass could address energy density concerns. Further, understanding the mechanisms behind gas evolution during aluminum dissolution is essential. Advanced characterization techniques, such as in-situ XPS or operando spectroscopy, could shed light on the Al-alloy interface, guiding the development of gas-suppressing coatings or additives.

Additionally, composite materials that combine UPD-modified alloys with electrochemical stabilization strategies, like hydrophobic or multifunctional coatings, could enhance both stability and energy density. The exploration of hybrid electrolytes, which balance the characteristics of aqueous and ionic liquid systems, may also offer promising advancements in the performance of aluminum alloy anodes.

Investigations into the effect of microstructural properties, such as grain size and morphology, can further refine the performance of these anodes. By tailoring the microstructure, researchers can minimize defects that lead to inefficiencies and enhance both the mechanical and chemical integrity of the anode during cycling. Through a combination of these strategies, it is possible to develop alloy and glassy metal anodes that optimize performance while maintaining the essential metrics of energy density and stability in aqueous aluminum batteries.

Overall, substantial knowledge gaps and ongoing debates persist concerning the strategies for stabilizing aluminum metal anodes in aqueous electrolytes and the underlying reaction mechanisms. A thorough and critical investigation is necessary to gain deeper insights, which are essential for enabling the practical implementation of modified aluminum metal anodes in aqueous battery systems.

Electrolyte & cathode design

Batteries can be conceptualized as reservoirs of interconnected chemical reactions; thus, an integrated and holistic approach is essential when designing advanced battery systems. In the case of aqueous Al batteries, the stability of the anode-electrolyte interface poses significant challenges. However, it is equally critical to recognize the importance of electrolytes and cathodes, both of which play pivotal roles in determining the overall electrochemical performance of the system.

Aqueous electrolytes, particularly those with low pH values, present unique challenges by increasing proton activity, which in turn enhances HER during aluminum nucleation [57]. Moreover, the high energy barrier associated with breaking H_2O–Al^{3+} bonds in the hexa-aqua complex results in sluggish Al deposition kinetics. To address these issues, advancements in aqueous electrolyte formulations must focus on several key areas. First, achieving a neutral or weakly acidic pH is crucial to mitigate HER and promote stable aluminum redox reactions. Second, altering the solvation structure of the H_2O–Al^{3+} complex through the incorporation of suitable salts, additives, or co-solvents can significantly enhance electrochemical stability. Tailoring the electrolyte composition to optimize ion transport and reduce the energy barriers for Al deposition is essential for improving the overall efficiency and longevity of aqueous Al batteries.

The selection of cathode materials is equally critical in the development of practical, grid-scale ESSs. Ideal cathode materials must not only possess high energy density and excellent conductivity, but also demonstrate chemical and structural compatibility with the aqueous electrolyte and aluminum anode. In addition, cathodes should exhibit resilience in the aqueous environment, maintaining their structural integrity over extended cycling. Current research has primarily focused on metal oxides, conducting polymers, and organic compounds; however, the discovery and development of novel cathode materials are necessary to further enhance battery performance. Cathode materials that provide a high average discharge voltage, specific capacity, and long-term cycling stability are essential to achieving the energy density and durability required for grid-scale applications.

Ultimately, future research should pursue an integrated approach, balancing improvements in anode stabil-

ity, electrolyte formulation, and cathode material development to realize the full potential of aqueous aluminum batteries for large-scale energy storage solutions.

Practical demonstrations

As previously discussed, the primary objective of aqueous batteries is to enable large-scale energy storage, ranging from GW- to TW-levels, at a low cost while ensuring enhanced safety. To achieve this, it is imperative that the performance of aqueous aluminum full-cells be rigorously assessed under realistic operating conditions that mirror practical applications. However, most studies to date have been limited to lab-scale demonstrations utilizing milliwatt-hour (mWh)-level coin cells, typically featuring an excess aluminum anode. While these setups are valuable for evaluating the fundamental electrochemical characteristics of individual battery components, they do not accurately reflect the complexities of full-scale systems. The reduced scale often minimizes the occurrence and detection of side reactions, which can be more pronounced in larger systems.

In order to advance aqueous Al-metal batteries toward real-world applications, a comprehensive evaluation of key factors essential for scaling up the technology is required. One of the most critical aspects is the N:P ratio (anode to cathode capacity ratio) of the full-cell, as an optimized ratio is necessary to achieve balanced and efficient charge/discharge cycles. Additionally, scaling up the cell design itself—from small coin cells to larger pouch or prismatic cells—presents challenges related to uniformity in material distribution, heat management, and mechanical integrity. Another essential consideration is the operating temperature, as elevated temperatures may exacerbate unwanted side reactions or degradation, while lower temperatures may slow reaction kinetics. Furthermore, practical applications require testing at higher current densities to ensure that the cells can deliver high power output while maintaining stable operation over extended cycling.

Beyond these factors, considerations such as electrolyte composition, pressure tolerance, and long-term cycling performance must be critically assessed as part of the scaling-up process. Only by addressing these scaling challenges can aqueous aluminum batteries transition from promising lab-scale systems to practical solutions capable of meeting the demands of grid-scale energy storage.

Perspectives

In conclusion, aqueous Al-metal batteries offer a compelling, cost-effective, and safer alternative to conventional LIBs for grid-scale ESSs. Their potential to address the growing demand for efficient and sustainable energy storage, particularly in the integration of renewable energy, is substantial. However, to fully realize the

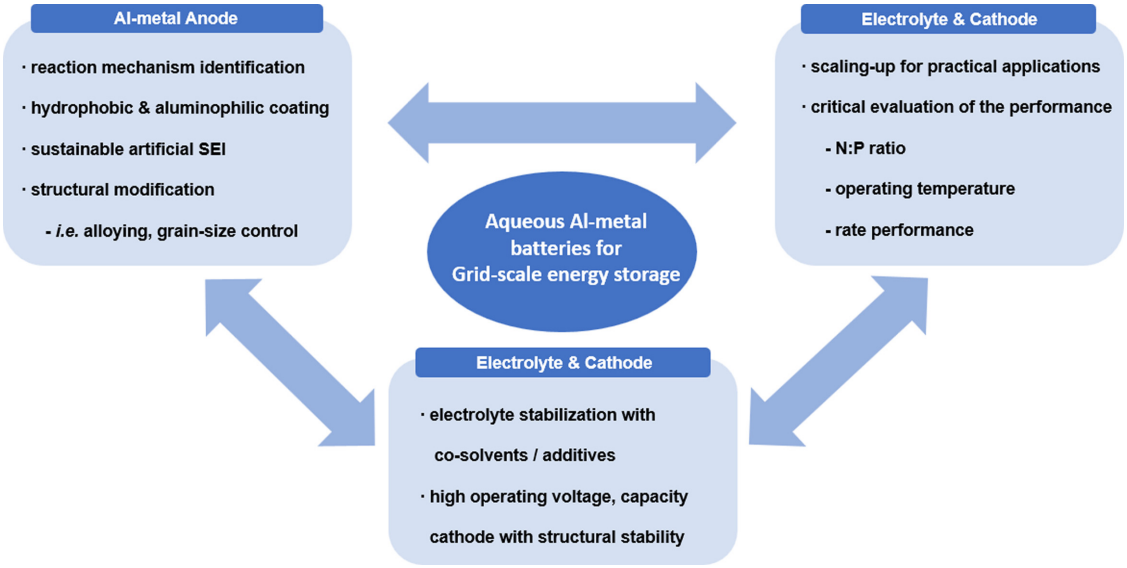

Fig. 10. Schematic illustration of the strategies for the development of practical aqueous Al-metal batteries for grid-scale energy storage.

potential of aqueous Al-metal batteries, future research must focus on developing tailored frameworks that account for the unique characteristics of this system, rather than relying on protocols designed for other battery technologies.

A critical challenge lies in unraveling the complexities of the aluminum plating/stripping mechanism in aqueous environments. Gaining a deeper understanding of this process is essential for overcoming current limitations and enabling the full potential of this technology. Once the fundamental reaction mechanisms are well understood, a comprehensive and multifaceted approach will be required to drive further advancements. This includes the development of effective strategies for anode protection, stabilization of electrolytes against decomposition, and the identification and optimization of suitable cathode materials that complement the electrochemical properties of aluminum in aqueous systems.

Addressing these challenges is crucial for scaling aqueous Al-metal batteries from laboratory-scale milliwatt-hour demonstrations to practical, large-scale applications. By overcoming these technical barriers, aqueous Al-metal batteries could become a transformative solution, contributing to the advancement of reliable and sustainable grid-scale energy storage.

ACKNOWLEDGMENTS

This research was supported by the Gachon University research fund of 2023 (GCU-202400930001).

REFERENCES

[1] N. S. Lewis, MRS Bulletin, 2007, 32, 808–820.
[2] IEA, Key World Energy Statistics 2015, International energy agency, Paris, 2015.
[3] D. Larcher and J.-M. Tarascon, Nat. Chem., 2015, 7, 19–29.
[4] IRENA, Global Energy Transformation: A Roadmap to 2050, International Renewable Energy Agency, Abu Dhabi, 2018.
[5] E. Barbour, I. A. G. Wilson, J. Radcliffe, Y. Ding, and Y. Li, Renew. Sustain. Energy Rev., 2016, 61, 421–432.
[6] B. Dunn, H. Kamath, and J.-M. Tarascon, Science, 2011, 334, 928–935.
[7] B. Bolund, H. Bernhoff, and M. Leijon, Renew. Sustain. Energy Rev., 2007, 11(2), 235–258.
[8] Precedence Research, Energy Storage Systems Market Size, Share, and Trends 2024 to 2034, 2022.
[9] U. Herrmann, B. Kelly, and H. Price, Energy, 2004, 29(5–6), 883–893.
[10] B. E. Conway, J. Electrochem. Soc., 1991, 138, 1539–1548.
[11] J. A. Turner, Science, 2004, 305, 972–974.
[12] X. Ji, Energy Environ. Sci., 2019, 12, 3203–3224.
[13] M. Li, J. Lu, Z. Chen, and K. Amine, Adv. Mater., 2018, 30(33), 1800561.
[14] S. Chu, and A. Majumdar, Nature, 2012, 488, 294–303.
[15] L. Lu, X. Han, J. Li, J. Hua, and M. Ouyang, J. Power Sources, 2013, 226, 272–288.
[16] A. Basile, M. Hilder, F. Makhlooghiazad, C. Pozo-Gonzalo, D. R. MacFarlane, P. C. Howlett, and M. Forsyth, Adv. Energy Mater., 2018, 8(17), 1703491.
[17] P. Ribière, S. Grugeon, M. Morcrette, S. Boyanov, S. Laruelle, and G. Marlair, Energy Environ. Sci., 2012, 5(1), 5271–5280.
[18] Y. Chen, Y. Kang, Y. Zhao, L. Wang, J. Liu, Y. Li, Z. Liang, X. He, X. Li, N. Tavajohi, and B. Li, J. Energy Chem., 2021, 59(8), 83–99.
[19] K. Chayambuka, G. Mulder, D. L. Danilov, and P. H. L. Notten, Adv. Energy Mater., 2020, 10(38), 2001310.
[20] Q. Wang, B. Mao, S. I. Stoliarov, and J. Sun, Prog. Energy Combust. Sci., 2019, 73, 95–131.
[21] G. Zubi, R. Dufo-López, M. Carvalho, and G. Pasaoglu, Renew. Sustain. Energy Rev., 2018, 89, 292–308.
[22] X. Wang, E. Yasukawa, and S. Kasuya, J. Electrochem. Soc., 2001, 148, A1066–A1071.
[23] K. Xu, S. Zhang, J. L. Allen, and T. R. Jow, J. Electrochem. Soc., 2002, 149, A1079–A1082.
[24] M. Armand, F. Endres, D. R. MacFarlane, H. Ohno, and B. Scrosati, Nat. Mater., 2009, 8, 621–629.
[25] B. Garcia, S. Lavallée, G. Perron, C. Michot, and M. Armand, Electrochim. Acta, 2004, 49(26), 4583–4588.
[26] A. Manthiram, X. Yu, and S. Wang, Nat. Rev. Mater., 2017, 2, 16103.
[27] Z. Gao, H. Sun, L. Fu, F. Ye, Y. Zhang, W. Luo, and Y. Huang, Adv. Mater., 2018, 30(17), 1705702.
[28] D. Fenton, J. M. Parker, and P. V. Wright, Polymer, 1973, 14(11), 589.
[29] C. Yang, J. Chen, T. Qing, X. Fan, W. Sun, A. von Cresce, M. S. Ding, O. Borodin, J. Vantamanu, M. A. Schroeder, N. Eidson,

C. Wang, and K. Xu, Joule, 2017, 1(1), 122–132.
[30] L. Suo, O. Borodin, T. Gao, M. Olguin, J. Ho, X. Fan, C. Luo, C. Wang, and K. Xu, Science, 2015, 350, 938–943.
[31] M. Ue, H. Tokuda, T. Kawai, M. Yanagidate, and Y. Otake, ECS Trans., 2009, 16, 173.
[32] K. Takechi, Y. Kato, and Y. Hase, Adv. Mater., 2015, 27(15), 2501–2506.
[33] A. Basile, M. Hilder, F. Makhlooghiazad, C. Pozo-Gonzalo, D. R. MacFarlane, P. C. Howlett, and M. Forsyth, Adv. Energy Mater., 2018, 8(17), 1703491.
[34] K. Ishiguro, Y. Nakata, M. Matsui, I. Uechi, Y. Takeda, O. Yamamoto, and N. Imanishi, J. Electrochem. Soc., 2013, 160, A1690.
[35] D. Ren, X. Feng, L. Liu, H. Hsu, L. Lu, L. Wang, X. He, and M. Ouyang, Energy Storage Mater., 2021, 34, 563–573.
[36] Q. Wang, P. Ping, X. Zhao, G. Chu, J. Sun, and C. Chen, J. Power Sources, 2012, 208, 210–224.
[37] M. Henriksen, K. Vågsæther, J. Lundberg, S. Forseth, and D. Bjerketvedt, J. Hazard. Mater., 2019, 371, 1–7.
[38] D. Chao, W. Zhou, F. Xie, C. Ye, H. Li, M. Jaroniec, and S.-Z. Qiao, Sci. Adv., 2020, 6, eaba4098.
[39] L. E. Blanc, D. Kundu, and L. F. Nazar, Joule, 2020, 4(4), 771–799.
[40] H. Jia, Z. Wang, B. Tawiah, Y. Wang, C.-Y. Chan, B. Fei, and F. Pan, Nano Energy, 2020, 70, 104523.
[41] L. Butterwick and G. D. W. Smith, Resour. Conserv. Recycl., 1986, 9(3), 281–292.
[42] Y. Ru, S. Zheng, H. Xue, and H. Pang, Chem. Eng. J., 2020, 382, 122853.
[43] T. Nagaura, 4th International Rechargeable Battery Seminar, Deerfield Beach, FL, USA, 1990.
[44] T. Nagaura and H. Shimotake (Ed.), Progress in Batteries and Solar Cells, JEC Press, US, 1990, 209–217.
[45] M. Winter, K.-C. Moeller, and J. O. Besenhard, Carbonaceous and graphitic anodes, In: G. A. Nazri and G. Pistoia (eds), Lithium Batteries, Springer, Boston, MA, 2003, 145–194.
[46] Y. Zhao, X. Li, B. Yan, D. Xiong, D. Li, S. Lawes, and X. Sun, Adv. Energy Mater., 2016, 6(8), 1502175.
[47] S. Liu, G. L. Pan, G. R. Li, and X. P. Gao, J. Mater. Chem. A, 2015, 3, 959–962.
[48] H. Lahan, R. Boruah, A. Hazarika, and S. K. Das, J. Phys. Chem. C, 2017, 121(47), 26241–26249.
[49] H. Lahan and S. K. Das, J. Power Sources, 2019, 413, 134–138.
[50] M. Hulot, CR Hebd. Acad. Sci, 1855, 40, 1148.
[51] D. Tommasi, Traité Théorique Et Pratique d'Électrochimie, George Carre, Paris, 1889, 131.
[52] C. H. Brown, Galvanic Battery, US Patent 503,567, 1893.
[53] S. Ruben, Primary cell, US Patent 2,638,489, 1953.
[54] S. Zaromb, J. Electrochem. Soc., 1962, 109, 1125.
[55] D. Peramunage, R. Dillon, and S. Licht, J. Power Sources, 1993, 45(3), 311–323.
[56] N. Jayaprakash, S. K. Das, and L. A. Archer, Chem. Commun., 2011, 47, 12610–12612.
[57] M.-C. Lin, M. Gong, B. Lu, Y. Wu, D.-Y. Wang, M. Guan, M. Angell, C. Chen, J. Yang, B.-J. Hwang, and H. Dai, Nature, 2015, 520, 324–328.
[58] D. J. Kim, D.-J. Yoo, M. T. Otley, A. Prokofjevs, C. Pezzato, M. Owczarek, S. J. Lee, J. W. Choi, and J. F. Stoddart, Nat. Energy, 2019, 4, 51–59.
[59] Z. Lin, M. Mao, C. Yang, Y. Tong, Q. Li, J. Yue, G. Yang, Q. Zhang, L. Hong, X. Yu, L. Gu, Y.-S. Hu, H. Li, X. Huang, L. Suo, and L. Chen, Sci. Adv., 2021, 7, eabg6314.
[60] Q. Pang, J. Meng, S. Gupta, X. Hong, C. Y. Kwok, J. Zhao, Y. Jin, L. Xu, O. Karahan, Z. Wang, S. Toll, L. Mai, L. F. Nazar, M. Balasubramanian, B. Narayanan, and D. R. Sadoway, Nature, 2022, 608, 704–711.
[61] Y. Guo, W. Wang, H. Lei, M. Wang, and S. Jiao, Adv. Mater., 2022, 34(13), 2110109.
[62] G. R. Pastel, Y. Chen, T. P. Pollard, M. A. Schroeder, M. E. Bowden, A. Zheng, N. T. Hahn, L. Ma, V. Murugesan, J. Ho, M. Garaga, O. Borodin, K. Mueller, S. Greenbaum, and K. Xu, Energy Environ. Sci., 2022, 15, 2460–2469.
[63] X. Wang, Z. Xi, and Q. Zhao, Ind. Chem. Mater., 2024, Advance Article.
[64] T. Dong, K. L. Ng, Y. Wang, O. Voznyy, and G. Azimi, Adv. Energy Mater., 2021, 11(20), 2100077.
[65] Z. Tong, R. Lian, R. Yang, T. Kang, J. Feng, D. Shen, Y. Wu, X. Cui, H. Wang, Y. Tang, and C.-S. Lee, Energy Storage Mater., 2022, 44, 497–507.
[66] M. Trachtman, G. D. Markham, J. P. Glusker, P. George, and C. W. Bock, Inorg. Chem., 1998, 37(17), 4421–4431.
[67] F. Xiao, R. Yang, and Z. Liu, Int. J. Hydrogen Energy., 2022, 47(1), 365–386.
[68] Z. Zhao, Z. Zhang, T. Xu, W. Wang, B. Wang, and X. Yu, J. Am. Chem. Soc., 2024, 146(3), 2257–2266.
[69] R. Tao, C. Gao, E. Xie, B. Wang, and B. Lu, Chem. Sci., 2022, 13, 10066–10073.
[70] W. Huang, K. Zhang, B. Yuan, L. Yang, and M. Zhu, Energy Storage Mater., 2022, 50, 152–160.
[71] L. T. Hieu, S. So, I. T. Kim, and J. Hur, Chem. Eng. J., 2021, 411, 128584.
[72] Q. Hao, F. Chen, X. Chen, Q. Meng, Y. Qi, and N. Li, Electrochim. Acta, 2022, 421, 140495.

[73] Y.-X. Yu, J. Phys. Chem. C, 2016, 120(10), 5288–5296.

[74] H. Yan, W. Li, H. Li, X. Fan, and M. Zhu, Prog. Org. Coat., 2019, 135, 156–167.

[75] X. Zhu, X. Li, M. L. K. Essandoh, J. Tan, Z. Cao, X. Zhang, P. Dong, P. M. Ajayan, M. Ye, and J. Shen, Energy Storage Mater., 2022, 50, 243–251.

[76] L. Yao, S. Ju, T. Xu, W. Wang, and X. Yu, ACS Nano, 2023, 17(24), 25027–25036.

[77] Q. Zhao, M. J. Zachman, W. I. Al Sadat, J. Zheng, L. F. Kourkoutis, and L. A. Archer, Sci. Adv., 2018, 4, eaau8131.

[78] R. Bai, J. Yang, G. Li, J. Luo, and W. Tang, Energy Storage Mater., 2021, 41, 41–50.

[79] S. Kumar, T. Salim, V. Verma, W. Manalastas Jr, and M. Srinivasan, Chem. Eng. J., 2022, 435, 134742.

[80] K. Nakayama, H. Miki, T. Nakagawa, K. Noi, Y. Sugawara, S. Kobayashi K. Sakurai, H. Iba, A. Kuwabara, Y. Ikuhara, and T. Abe, J. Mater. Chem. A, 2024, 12, 8350–8358.

[81] B.-E. Jia, E. Hu, Z. Hu, J. J. Liew, Z. Hong, Y. Guo, M. Srinivasan, Q. Zhu, J. Xu, J. Chen, H. Pan, and Q. Yan, Energy Storage Mater., 2024, 65, 103141.

[82] C. B. Breslin and W. M. Carroll, Corros. Sci., 1992, 33(11), 1735–1746.

[83] H. Yu, C. Lv, C. Yan, and G. Yu, Small Methods, 2023, 8(6), 2300758.

[84] Q. Ran, H. Shi, H. Meng, S.-P. Zeng, W.-B. Wan, W. Zhang, Z. Wen, X.-Y. Lang, and Q. Jiang, Nat. Commun., 2022, 13, 576.

[85] A. Hirata, P. Guan, T. Fujita, Y. Hirotsu, A. Inoue, A. R. Yavari, T. Sakurai, and M. Chen, Nat. Mater., 2011, 10, 28–33.

[86] D. C. Hofmann, J.-Y. Suh, A. Wiest, G. Duan, M.-L. Lind, M. D. Demetriou, and W. L. Johnson, Nature, 2008, 451, 1085–1089.

[87] X. Wang, G. Pawar, Y. Li, X. Ren, M. Zhang, B. Lu, A. Banerjee, P. Liu, E. J. Dufek, J.-G. Zhang, J. Xiao, J. Liu, Y. S. Meng, and B. Liaw, Nat. Mater., 2020, 19, 1339–1345.

[88] Z. Jia, X. Duan, P. Qin, W. Zhang, W. Wang, C. Yang, H. Sun, S. Wang, and L.-C. Zhang, Adv. Funct. Mater., 2017, 27(38), 1702258.

[89] G. Wu, X. Zheng, P. Cui, H. Jiang, X. Wang, Y. Qu, W. Chen, Y. Lin, H. Li, X. Han, Y. Hu, P. Liu, Q. Zhang, J. Ge, Y. Yao, R. Sun, Y. Wu, L. Gu, X. Hong, and Y. Li, Nat. Commun., 2019, 10, 4855.

[90] C. Yan, C. Lv, B. E. Jia, L. Zhong, X. Cao, X. Guo, H. Liu, W. Xu, D. Liu, L. Yang, J. Liu, H. H. Hng, W. Chen, L. Song, S. Li, Z. Liu, Q. Yan, and G. Yu, J. Am. Chem. Soc., 2022, 144(25), 11444–11455.

[91] P. M. Natishan and W. E. O'grady, J. Electrochem. Soc., 2014, 161(9), C421.

[92] Y. Zhang, Y. Bian, Z. Lv, Y. Han, and M.-C. Lin, ACS Appl. Mater. Interfaces, 2021, 13(31), 37091–37101.

[93] Y.-H. Wu, W.-J. Lin, T.-H. Tsai, and M.-C. Lin, ACS Appl. Energy Mater., 2024, 7(9), 3957–3967.